AGU PUBLICATIONS

JGR

Journal of Geophysical Research: Solid Earth

RESEARCH ARTICLE

10.1002/2012JB010016

Key Points:
- Analytical models for heat transfer in fracture networks are derived
- Matrix diffusivity tensor is a key parameter controlling fracture temperature
- Classical models overestimate fracture temperature and time-to-equilibrium

Correspondence to:
D. M. Tartakovsky,
dmt@ucsd.edu

Citation:
Ruiz Martínez, Á., D. Roubinet, and D. M. Tartakovsky (2014), Analytical models of heat conduction in fractured rocks, *J. Geophys. Res. Solid Earth*, *119*, doi:10.1002/2012JB010016.

Received 29 DEC 2012
Accepted 11 DEC 2013
Accepted article online 16 DEC 2013

Analytical models of heat conduction in fractured rocks

Á. Ruiz Martínez[1], D. Roubinet[1], and D. M. Tartakovsky[1]

[1]Department of Mechanical and Aerospace Engineering, University of California, San Diego, La Jolla, California, USA

Abstract Discrete fracture network models routinely rely on analytical solutions to estimate heat transfer in fractured rocks. We develop analytical models for advective and conductive heat transfer in a fracture surrounded by an infinite matrix. These models account for longitudinal and transverse diffusion in the matrix, a two-way coupling between heat transfer in the fracture and matrix, and an arbitrary configuration of heat sources. This is in contrast to the existing analytical solutions that restrict matrix conduction to the direction perpendicular to the fracture. We demonstrate that longitudinal thermal diffusivity in the matrix is a critical parameter that determines the impact of local heat sources on fluid temperature in the fracture. By neglecting longitudinal conduction in the matrix, the classical models significantly overestimate both fracture temperature and time-to-equilibrium. We also identify the fracture-matrix Péclet number, defined as the ratio of advection timescale in the fracture to diffusion timescale in the matrix, as a key parameter that determines the efficiency of geothermal systems. Our analytical models provide an easy-to-use tool for parametric sensitivity analysis, benchmark studies, geothermal site evaluation, and parameter identification.

1. Introduction

Heat transfer in fractured rocks is a critical phenomenon that drives the performance of both enhanced geothermal systems (wherein the heat transferred from hot dry rocks warms water circulating in fractures) [*Willis-Richards et al.*, 1996; *Gelet et al.*, 2012] and enhanced oil recovery (wherein oil viscosity is reduced by injecting hot water or steam, thus increasing rock temperature) [*Al-Hadhrami and Blunt*, 2001]. Heat conduction impacts the structural properties of ambient rocks by creating new or reopening existing microfractures [*Wang et al.*, 1989; *Lin*, 2002] and/or modifying rock alteration patterns [*Xu and Pruess*, 2001]. Its negative effects are manifested in seismic activity induced by geothermal energy extraction [*Gunasekera et al.*, 2003; *Chen and Shearer*, 2011] and in nuclear waste leakage due to heat generated by radioactive decay [*Xiang and Zhang*, 2012; *Wang et al.*,1981].

Heat transfer in fractured subsurface environments takes place in at least two distinct phases: fluid-filled fractures and ambient solid matrix. Existing analytical and semianalytical models of heat conduction in fractured rocks consider single isolated fractures [*Meyer*, 2004] and networks of equally spaced horizontal [*Bodvarsson and Tsang*,1982] or vertical [*Yang and Yeh*, 2009; *Gringarten et al.*, 1975] fractures. It is important to recognize that single-fracture representations are important not only in their own right but also as conceptual representations of mobile/immobile regions in natural fractured systems [*Zhou et al.*, 2007]. Such models are amenable to the same mathematical treatment as their counterparts developed for mass transport in discrete fracture networks. Examples of the latter include analytical [*Tang et al.*, 1981], semianalytical [*Roubinet et al.*, 2012; *Sudicky and Frind*, 1982], and numerical [*Roubinet et al.*, 2010] models of solute transport due to advection and diffusion in fractures and pure diffusion in the host matrix. A key difference between heat and mass transfer in fractured environments is that heat readily diffuses through both solid and fluid phases, whereas solutes spread largely in the fluid phase. While potentially important [e.g., *Bataillé et al.*, 2006], investigation of variable-density flow and heat transport lies outside the scope of the present study.

Analytical solutions, such as those mentioned above, provide significant physical insight into these transport phenomena and act as an invaluable component in field-scale screening and management (decision support) models. Yet they rely on a number of simplifying assumptions that might not be valid in a specific application. While these solutions routinely neglect longitudinal diffusion in the matrix, its impact on heat and mass transfer can be significant [*Molson et al.*, 2007; *Roubinet et al.*, 2012]. Likewise, longitudinal diffusion in the matrix (which is typically neglected in analytical models) is an important mechanism of heat transfer in a system of several fractures [*Cheng et al.*, 2001; *Baston and Kueper*, 2009; *Kolditz*, 1995]. It can

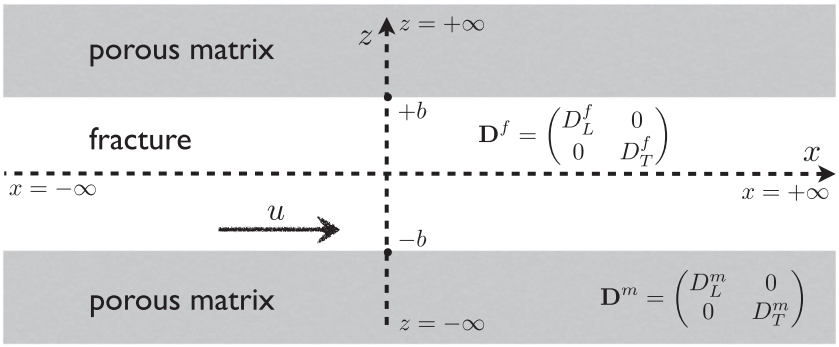

Figure 1. Single fracture embedded in an infinite matrix.

overestimate the thermal drawdown by up to 11% after 20 years of heat mining from HDRs in fractured crystalline rocks [*Kolditz*, 1995].

In the present study, we develop an analytical model of heat transfer in individual fractures, which accounts both for longitudinal and transverse diffusion in the matrix and for longitudinal and transverse dispersion and diffusion in the fracture. Section 2 provides a mathematical formulation of the problem. Section 3 contains its general solution in the Fourier-Laplace space. This solution is inverted analytically under conditions that are typical of most geothermal reservoirs (section 3.2). We compare our analytical solutions with their existing counterparts in section 4 and demonstrate their physical and practical implications in section 5. Major conclusions from our study are summarized in section 6.

2. Problem Formulation

Consider fluid flow and heat transfer in a fracture with aperture $2b$ and infinite length that is embedded in a homogeneous rock matrix with porosity ϕ (Figure 1). Following the standard practice in the field [e.g., *Kolditz*, 1995; *Cheng et al.*, 2001; *Baston and Kueper*, 2009; *Xiang and Zhang*, 2012], we assume the steady state flow to be single phase, incompressible, and laminar; the gravity effects and density variation with temperature to be negligible; and the fracture walls to be smooth and parallel to each other. Some of these assumptions can be relaxed, as discussed in the concluding remarks in section 6. Since the problem is symmetric about the plane $z = 0$, we restrict our analysis to the upper half of the computational domain, so that the fracture is represented by $\Omega_f = \{(x,z) : -\infty < x < \infty, 0 \le z \le b\}$ and the matrix by $\Omega_m = \{(x,z) : -\infty < x < \infty, b \le z < \infty\}$. Fluid temperature in the fracture, $T^f(x,z,t)$, satisfies an advection-dispersion equation

$$\frac{\partial T^f}{\partial t} + u\frac{\partial T^f}{\partial x} = D_L^f \frac{\partial^2 T^f}{\partial x^2} + D_T^f \frac{\partial^2 T^f}{\partial z^2} + f, \quad \mathbf{x} \in \Omega_f \tag{1}$$

where $\mathbf{x} = (x,z)^\top$ is the position vector, u is the fluid velocity, $f(\mathbf{x},t)$ is a source term, and D_L^f and D_T^f are the longitudinal and transverse dispersion coefficients, respectively. For a fluid of density ρ_f and heat capacity c_f, these are given by $D_L^f = \lambda_L^f/\alpha_f + E_L^f/\alpha_f$ and $D_T^f = \lambda_T^f/\alpha_f + E_T^f/\alpha_f$, where $\alpha_f = \rho_f c_f$, λ_L^f and λ_T^f are the longitudinal and transverse thermal conductivity coefficients, and E_L^f and E_T^f the longitudinal and transverse thermal dispersion coefficients [*Yang and Yeh*, 2009].

The ambient matrix Ω_m is assumed to be impervious to flow. The heat spreads throughout the matrix by conduction, so that temperature in the matrix, $T^m(\mathbf{x},t)$, is governed by a diffusion equation

$$\frac{\partial T^m}{\partial t} = D_L^m \frac{\partial^2 T^m}{\partial x^2} + D_T^m \frac{\partial^2 T^m}{\partial z^2}, \quad \mathbf{x} \in \Omega_m, \tag{2}$$

where $D_L^m = \lambda_L^e/c_e$ and $D_T^m = \lambda_T^e/c_e$ are the longitudinal and transverse diffusion coefficients, c_e is the effective heat capacity of the matrix, and λ_L^e and λ_T^e the longitudinal and transverse thermal conductivity coefficients in the matrix.

Let $T_i(x,z)$ denote the initial temperature in the system. Then equations (1) and (2) are subject to initial conditions

$$T^f(x,z,0) = T_i(x,z), \qquad T^m(x,z,0) = T_i(x,z). \tag{3}$$

Equation (1) is subject to boundary conditions

$$T^f(\pm\infty, z, t) = T_i, \quad \frac{\partial T^f}{\partial z}(x, 0, t) = 0, \tag{4}$$

and equation (2) to boundary conditions

$$T^m(\pm\infty, z, t) = T_i, \quad T^m(x, \infty, t) = T_i. \tag{5}$$

At the fracture-matrix interface $z = b$, both the temperature and the heat flux are continuous, giving rise to two interfacial conditions

$$T^f = T^m, \qquad \phi_m D_T^m \frac{\partial T^m}{\partial z} = D_T^f \frac{\partial T^f}{\partial z} \equiv r, \qquad z = b, \tag{6}$$

where $\phi_m = \phi + (1-\phi)\rho_s c_s/(\rho_f c_f)$; ρs and cs are the density and heat capacity of the solid phase, respectively; and $r(x, t)$ is the (unknown) thermal flux between the fracture and matrix. Since the boundary value problems (BVPs) (1)–(6) are invariant under transformations $T = T^j - T_i$ ($j = f, m$), we set, without loss of generality, $T_i = 0$.

In what follows, we first develop general solutions of BVPs (1)–(6), which are applicable to a wide range of source functions $f(\mathbf{x}, t)$. Then we proceed by analyzing these solutions in detail for f representing a point injection of heat at $x = 0$. This setting is relevant to both natural and forced convection. For example, it represents fluid injection through a well that intersects a fracture at $x = 0$. If the temperature of the injected fluid is appreciably different from the initial temperature T_i of the host fluid, then this setup can be used to characterize fractured rocks by collecting temperature logs at the well; *Pehme et al.* [2007, 2010] used it to detect the presence of active fractures under natural groundwater flow conditions. Another example described by the model is an enhanced geothermal system, in which the fluid velocity u is induced by, e.g., groundwater extraction at point $x = x_i > 0$. If the fracture fluid is at the initial temperature T_i, the objective is to evaluate how the temperature of the fluid extracted at $x = x_i$ is modified by warmer/colder water injected at $x = 0$ under forced flow conditions.

3. Analytical Solutions

The fracture BVP consists of (1), (3), (4) and the second condition in (6). The matrix BVP is composed of (2), (3), (5) and the second condition in (6). Let $G^f(x, z; x', z'; t - t')$ and $G^m(x, z; x', z'; t - t')$ denote the Green's functions associated with the fracture and matrix BVPs, respectively. Their analytical expressions are given in Appendix A.

Our analytical models are first derived in the Fourier-Laplace (FL) space. For any suitable function $A(x, t)$, we define its Laplace and Fourier transformations as

$$\bar{A}(x, s) = \int_0^\infty A(x, t)\mathrm{e}^{-st}\mathrm{d}t, \tag{7a}$$

$$\tilde{A}(\xi, s) = \frac{1}{\sqrt{2\pi}} \int_{-\infty}^{\infty} \bar{A}(x, s)\mathrm{e}^{-ix\xi}\mathrm{d}x. \tag{7b}$$

3.1. General Solution in Fourier-Laplace Space

We show in Appendix B that the FL transforms of the temperature in the fracture, $\tilde{T}^f(\xi, z, s)$, and matrix, $\tilde{T}^m(\xi, z, s)$, are given by

$$\tilde{T}^f = \sqrt{2\pi}\left[\frac{F_1(\xi, s)\Delta\mathcal{F}(b; \xi; s)}{F_2(\xi, s) + 1/\beta} - \Delta\mathcal{F}(z; \xi; s)\right] \tag{8}$$

and

$$\tilde{T}^m = -\frac{\sqrt{2\pi}}{\beta}\exp\left(-\frac{\psi|z-b|}{\sqrt{D_T^m}}\right)\frac{\Delta\mathcal{F}(b; \xi; s)}{F_2(\xi, s) + 1/\beta}. \tag{9}$$

Here $\Delta\mathcal{F}(z;\xi;s) = \tilde{\mathcal{F}}(z,0;\xi;s) - \tilde{\mathcal{F}}(z,b;\xi;s)$, $\tilde{\mathcal{F}}(z,z';\xi;s)$ is the antiderivative of $\tilde{f}\tilde{G}^f$ with respect to z', $\psi = \sqrt{D_L^m\xi^2 + s}$, $\beta = \phi_m\sqrt{D_T^m}\psi$, and

$$F_1 = \frac{\tilde{G}^f_\xi(s)}{b} + \frac{2}{b}\sum_{n=1}^{\infty}(-1)^n\cos(\alpha_n z)\tilde{G}^f_\xi(s+\alpha_n^2 D_T^f) \tag{10a}$$

$$F_2 = \frac{\tilde{G}^f_\xi(s)}{b} + \frac{2}{b}\sum_{n=1}^{\infty}(-1)^{2n}\tilde{G}^f_\xi(s+\alpha_n^2 D_T^f) \tag{10b}$$

where $G^f_\xi(s)$ is given by (A4) and $\alpha_n = n\pi/b$.

The FL transform of the temperature distribution in the fracture-matrix system, (8) and (9), is free of any simplifying assumptions. It captures full (two-way) coupling of the fracture-matrix exchange and accounts for longitudinal and transverse dispersion and diffusion in the fracture and matrix, respectively. It also enables one to deal with arbitrary heat sources.

3.2. Explicit Models of Temperature in the Fracture

In the case of complete transverse mixing ($D_T^f = \infty$) and negligible longitudinal dispersion ($D_L^f = 0$) in the fracture, the general FL solutions (8) and (9) can be inverted analytically, yielding a closed-form expression for the temperature distribution. These conditions are typical for fracture-matrix systems. Indeed, the impact of longitudinal dispersion is limited to low velocities ($\leq 10^{-7}$ m/s) [*Tang et al.*, 1981], and transverse dispersion is important only if $D_T^f < D_T^m$ [*Roubinet et al.*, 2012].

Consider a continuous-in-time point source located at $x = 0$, such that $f = T_0 u\delta(x)\mathcal{H}(t)$, where T_0 is the temperature of the injected fluid (or the difference between the temperature of the injected fluid and its initial value T_i if the latter is not zero) and $\mathcal{H}(\cdot)$ is the Heaviside function. In the limit of $D_T^f \to \infty$ and $D_L^f \to 0$, (8) reduces to

$$\tilde{T}^f = \frac{1}{\sqrt{2\pi s}}\frac{T_0 u}{\beta/b + s + u\xi i}. \tag{11}$$

Let us define dimensionless ratio R, coefficient K, and critical time $t_{\min}$ as

$$R = \frac{\phi_m\sqrt{D_T^m D_L^m}}{ub}, \quad K = \frac{\phi_m}{2b}\sqrt{\frac{D_T^m}{D_L^m}}, \quad t_{\min} = \frac{10^4 b^2}{\phi_m^2 D_T^m}. \tag{12}$$

Note that since $\sqrt{D_T^m D_L^m}$ is the geometric mean of the heat diffusivity in the matrix and u/ϕ_m is a scaled advective velocity in the fracture, one can think of R as the inverse of a "fracture-matrix Péclet number" in that it represents a ratio of advection timescale in the fracture to diffusion timescale in the matrix. We show in Appendix C that for $R > 1$, $K > 1$, and $t > t_{\min}$, the inverse FL transformation of (11) yields

$$\begin{aligned} T^f(x,t) \sim & -\frac{T_0}{2\pi}\frac{R}{\mathcal{R}}\mathrm{Ei}\left(-\frac{1}{4t_d^*}\right) + \frac{T_0}{2}\frac{1}{\mathcal{R}}\left\{\mathrm{sgn}(x) - \mathrm{erf}\left[\frac{\mathrm{sgn}(x)}{2\sqrt{t_d^*}}\frac{R}{\sqrt{\mathcal{R}}}\right]\right\} \\ & + \frac{T_0}{\pi}\mathrm{e}^{-R^2/(4\mathcal{R}t_d^*)}\left\{-\frac{\sqrt{\pi t_d^*}}{2t_a^*}\frac{\mathrm{sgn}(x)}{R\sqrt{\mathcal{R}}} + \frac{2t_a^*-1}{2t_a^*\mathcal{R}^{3/2}} + \frac{2t_a^*-3}{12t_a^{*}\mathcal{R}^{5/2}}\right. \\ & + \frac{1}{\mathcal{R}^{7/2}}\left[\frac{R^2(1-2t_a^*)}{24t_d^* t_a^*} + \frac{3}{40t_a^*} - \frac{3}{16t_a^{*2}}\right] \\ & \left. + \frac{R^2(5-6t_a^*)}{80t_d^* t_a^{*2}\mathcal{R}^{9/2}} + \frac{R^4(2t_a^*-1)}{320t_d^{*2}t_a^{*2}\mathcal{R}^{11/2}}\right\} \end{aligned} \tag{13}$$

where $\mathcal{R} = R^2+1$ and $t_a^* = tu/x$ and $t_d^* = tD_L^m/x^2$ are the dimensionless advection and (longitudinal) diffusion times, respectively.

The conditions $R > 1$, $K > 1$, and $t > t_{\min}$ are adequate for geothermal studies: Typical thermal diffusivity in rocks is $D^m = \mathcal{O}(10^{-6}\mathrm{m}^2/\mathrm{s})$ [*Baston and Kueper*, 2009], and typical prediction times are larger than hours. Therefore, (13) provides a robust explicit prediction of spatiotemporal evolution of temperature in an infinite fracture. It accounts for both longitudinal and transverse diffusion in the matrix.

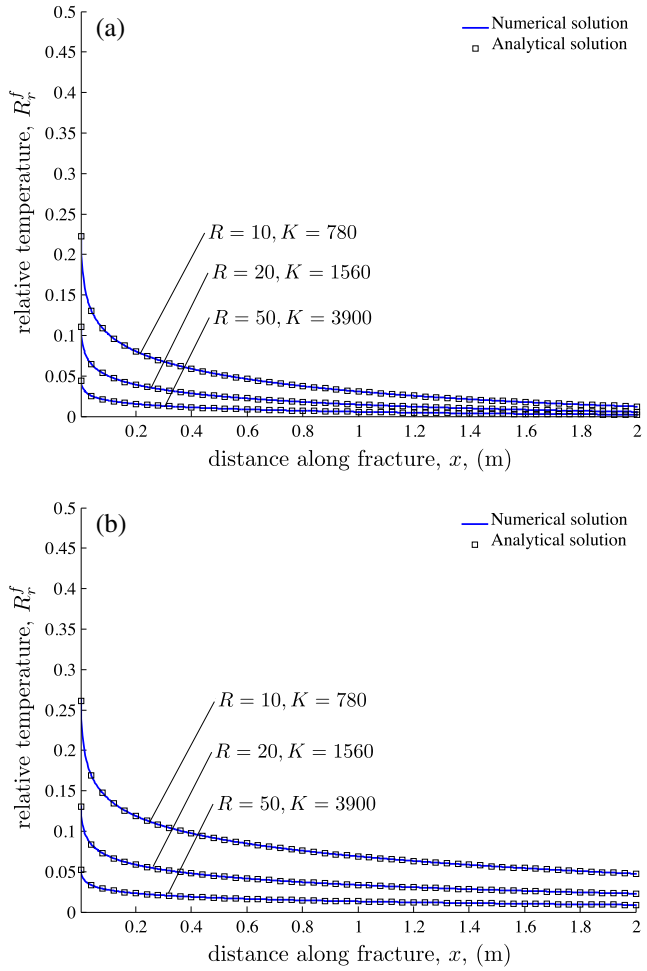

Figure 2. Distributions of the relative temperature along the fracture for flow velocity $u = 1.4 \times 10^{-4}$ m/s and different values of the dimensionless parameters R and K, computed with the analytical and numerical solutions. The liquid is injected at $x = 0$ during (a) $t = 1$ month and (b) $t = 1$ year.

In lieu of another example, we consider a pulse injection of duration t_p. This corresponds to the source term $f = T_0 u \delta(x)[\mathcal{H}(t) - \mathcal{H}(t - t_p)]$, and fracture temperature

$$T_p^f(x,t) = T^f(x,t)\mathcal{H}(t) - T^f(x,t-t_p)\mathcal{H}(t-t_p), \tag{14}$$

where $T^f(x,t)$ is given by (13).

3.3. Accuracy of Analytical Solutions

Our analytical solutions, e.g., (11), are exact in the Fourier-Laplace space. Their analytical inversion in Appendix C is approximate since it is based on truncation of the Taylor series involved. We assess the accuracy of the resulting analytical solutions, e.g., (13), by comparing them with their counterparts computed with numerical inversion of the corresponding expressions in the Fourier-Laplace space, e.g., (11). The latter is accomplished by using the *de Hoog et al.* [1982] algorithm and the MATLAB routine `ifft` to compute the inverse Laplace and Fourier transforms, respectively. In the simulations reported below we set $D_L^m = D_T^m = 9.16 \times 10^{-7}$ m^2/s, $\phi = 0.1$, $\rho_s = 2757$ kg/m^3, $c_s = 1180$ J/kgK and $\phi_m = 0.78$.

Figures 2 and 3 exhibit distributions of the relative fracture temperature $T_r^f = T^f/T_0$ for two transport configurations. The first (Figure 2) corresponds to flow with velocity $u = 1.4 \times 10^{-4}$ m/s in a fracture whose aperture is $2b = 1.0 \times 10^{-3}$, 5.0×10^{-4}, and 2.0×10^{-4} m or $R = 10$, 20, and 50. The second (Figure 3) corresponds to $u = 1.4 \times 10^{-3}$ m/s, and $2b = 1.0 \times 10^{-3}$, 5.0×10^{-4}, and 2.0×10^{-4} m or $R = 1$, 2 and 5. Both cases demonstrate the agreement between the analytical and numerical solutions for $t = 1$ month (Figures 2a and 3a) and 1 year (Figures 2b and 3b), which is to be expected since the conditions of validity of our solutions are

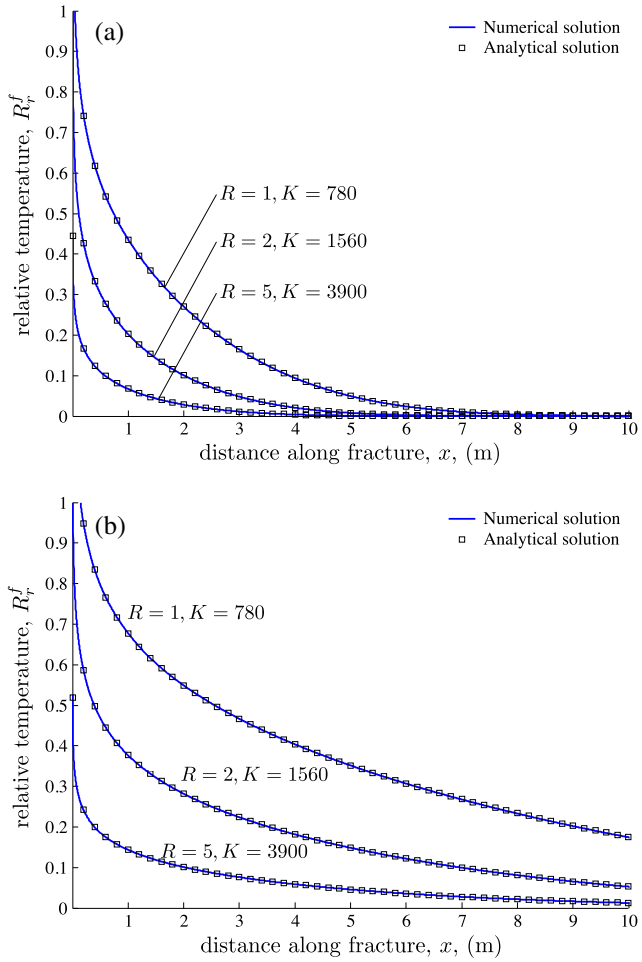

Figure 3. Distributions of the relative temperature along the fracture for flow velocity $u = 1.4 \times 10^{-3}$ m/s and different values of the dimensionless parameters R and K, computed with the analytical and numerical solutions. The liquid is injected at $x = 0$ during (a) $t = 1$ month and (b) $t = 1$ year.

fulfilled. Although not shown here, this agreement deteriorates for $R < 1$, a condition that is rarely (if ever) met in the field (see the discussion in the previous section).

4. Comparison With Existing Models

In this section we demonstrate that under certain conditions/assumptions our solutions reduce to the classical solutions of *Tang et al.* [1981] for semi-infinite fractures.

4.1. No Dispersion in Semi-Infinite Fracture

Setting $D_L^f = 0$, $D_L^m = 0$, and $D_T^f \to \infty$ (the complete mixing assumption) reduces our general solution (8) to

$$\tilde{T}^f = -\frac{\Delta\mathcal{F}(z;\xi;s)}{\alpha_s + u\xi i} \tag{15}$$

where $\alpha_s = \phi_m\sqrt{D_T^m s}/b + s$. For a point injection of fluid with temperature T_0, i.e., for $f = T_0 u\delta(x)\mathcal{H}(t)$, this gives rise to the Laplace transform of temperature in the fracture,

$$\bar{T}^f = \frac{T_0}{s}\exp\left(-\frac{\alpha_s x}{u}\right), \qquad x \geq 0. \tag{16}$$

This is identical to the analytical solution [*Tang et al.*, 1981] for heat transfer in a semi-infinite fracture with a fixed temperature T_0 at the fracture's inlet $x = 0$. This solution ignores longitudinal dispersion in the fracture and is referred to by *Tang et al.* [1981] as "transient solution with $D = 0$".

4.2. Longitudinal Dispersion in Semi-Infinite Fracture

Setting $D_L^m = 0$ and $D_T^f \to \infty$ reduces our general solution (8) to

$$\bar{T}^f = -\frac{\Delta\mathcal{F}(z;\xi;s)}{\alpha_s + D_L^f\xi^2 + u\xi i}. \tag{17}$$

The "general transient solution" of *Tang et al.* [1981] is recovered from (17) by choosing the source term to be

$$\bar{f} = \frac{T_0}{s}\sqrt{u^2 + 4D_L^f\alpha_s}\,\delta(x). \tag{18}$$

This choice accounts for the "lost" part of the injected flux due to the longitudinal diffusion in the negative half ($-\infty < x < 0$) of the infinite fracture. The resulting Laplace transform of temperature in the fracture is

$$\bar{T}^f = \frac{T_0}{s}\exp\left[-\left(\sqrt{\frac{u^2}{4} + D_L^f\alpha_s} - \frac{u}{2}\right)\frac{x}{D_L^f}\right], \quad x \geq 0. \tag{19}$$

5. Results and Discussion

The subsequent discussion serves to demonstrate the importance of accounting for two-dimensional heat conduction in rock matrix. In this discussion, we refer to (13) and (16) as "2-D solution" and "1-D solution," respectively.

The results below correspond to continuous point injection ($x = 0$) of a fluid whose temperature T_0 is either warmer ($T_0 > 0$) or colder ($T_0 < 0$) than the host fluid (the initial temperature $T_i = 0$). Unless specified otherwise, a shale matrix has the following characteristics: $D_L^m = D_T^m = 9.16\times10^{-7}$ m^2/s, $\phi = 0.1$, $\rho_s = 2757$ kg/m^3, and $c_s = 1180$ J/kg K. Taking the fluid to be water ($\rho_f = 1070$ kg/m^3 and $c_f = 4050$ J/kg K) yields $\phi_m = [\phi + (1-\phi)\rho_s c_s/(\rho_f c_f)] = 0.78$.

The results are reported in terms of the relative fracture temperature

$$T_r^f(x,t) = T^f(x,t)/T_0, \tag{20}$$

which ranges from 0 (temperature is at its initial value T_i) to 1 (temperature at the local heat source).

5.1. Effects of Heat Conduction in Matrix

Figure 4 depicts the temporal evolution of relative temperature T_r^f at the distance $x = 0.5$ m from the heat source. Flow velocity in the fracture is set to $u = 1.4\times10^{-4}$ m/s, and fracture aperture to $2b = 2\times10^{-4}$ m (Figure 4a), 5×10^{-4} m (Figure 4b), and 10^{-3} m (Figure 4c). This choice of fracture apertures yields the values of the dimensionless ratio $R = 50$ (Figure 4a), $R = 20$ (Figure 4b), and $R = 10$ (Figure 4c).

In the diffusion-dominated regime (Figure 4a), the 1-D solution (no longitudinal heat conduction in the matrix) underestimates the relative temperature at short times and significantly overestimates it at later times. The longitudinal heat conduction in the matrix (the 2-D solution) causes the fracture temperature to rise at earlier times and shows that the local heat source impacts on the fracture temperature ($T_r^f > 0$) at much earlier times; after this initial time interval, the 1-D solution predicts a much larger rate of increase of the fracture temperature than the 2-D solutions do. This is because heat is transferred from the fracture into the matrix in the vicinity of the localized injection, diffuses longitudinally in the matrix, and then returns to the fracture at locations far from the injection. Our 2-D solution captures this heat transfer mechanism in the diffusion-dominated regime, while the classical 1-D solution does not. Figures 4b and 4c show that this mechanism does not occur in advection-dominated regimes.

In all heat transfer regimes (Figures 4a–4c), both temperature in the fracture and the time-to-equilibrium increase as the matrix diffusion coefficient D_L^m decreases. The smaller the value of R (i.e., the larger the fracture-matrix Péclet number), the more pronounced this effect becomes. Ignoring longitudinal diffusion in the matrix (the 1-D solution) significantly underestimates the fracture-matrix transfer and significantly overestimates both temperature in the fracture and the time-to-equilibrium.

Overestimation of the time-to-equilibrium has important practical implications, since determination of the time it takes a fracture-matrix system to reach thermal equilibrium (steady state) is essential for estimation of the matrix penetration depth. The latter determines the adequacy of conceptual representations of

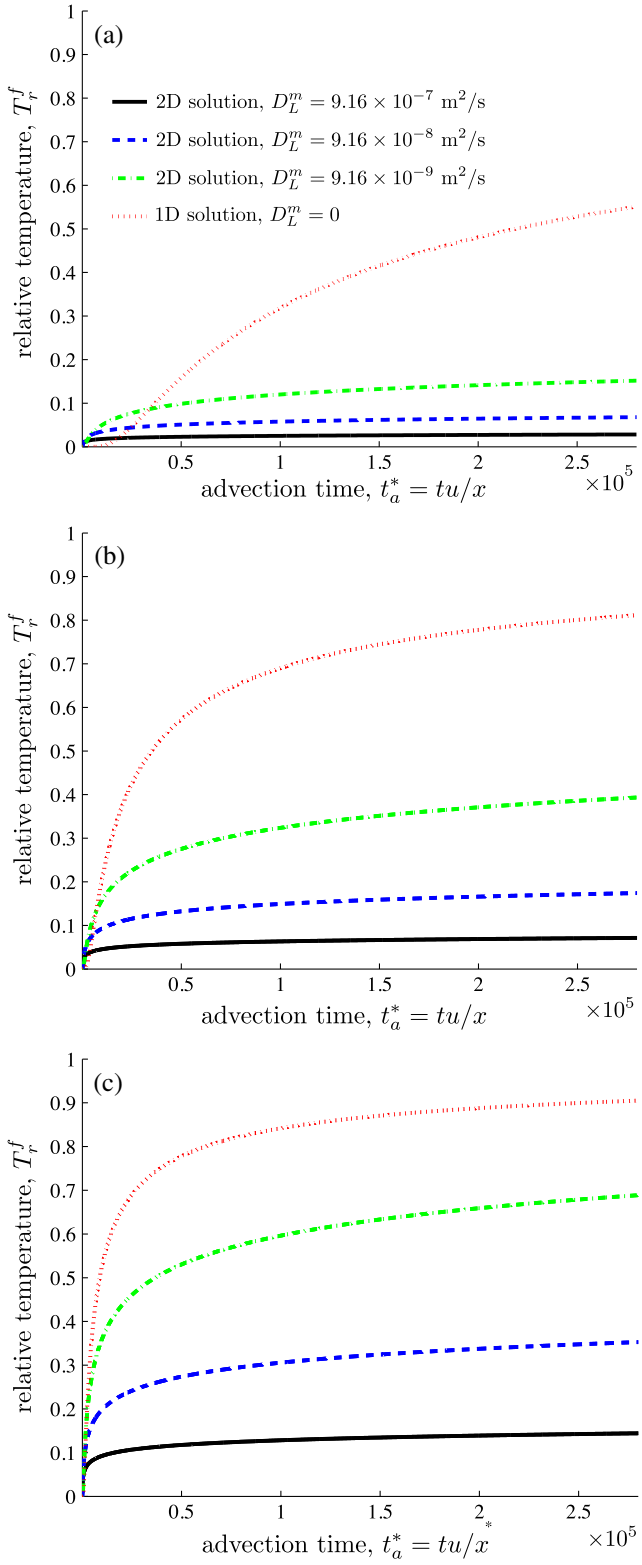

Figure 4. Relative temperature in the fracture T_r^f, as a function of advection time $t_a^* = tu/x$, computed with the 1-D solution (red dotted lines) and the 2-D solution for $D_L^m = 9.16 \times 10^{-9}$ (green dash-dotted lines), 9.16×10^{-8} (blue dashed lines), and 9.16×10^{-7} m^2/s (black solid lines). Fracture aperture $2b$ is set to (a) 2×10^{-4} m, (b) 5×10^{-4} m, and (c) 10^{-3} m.

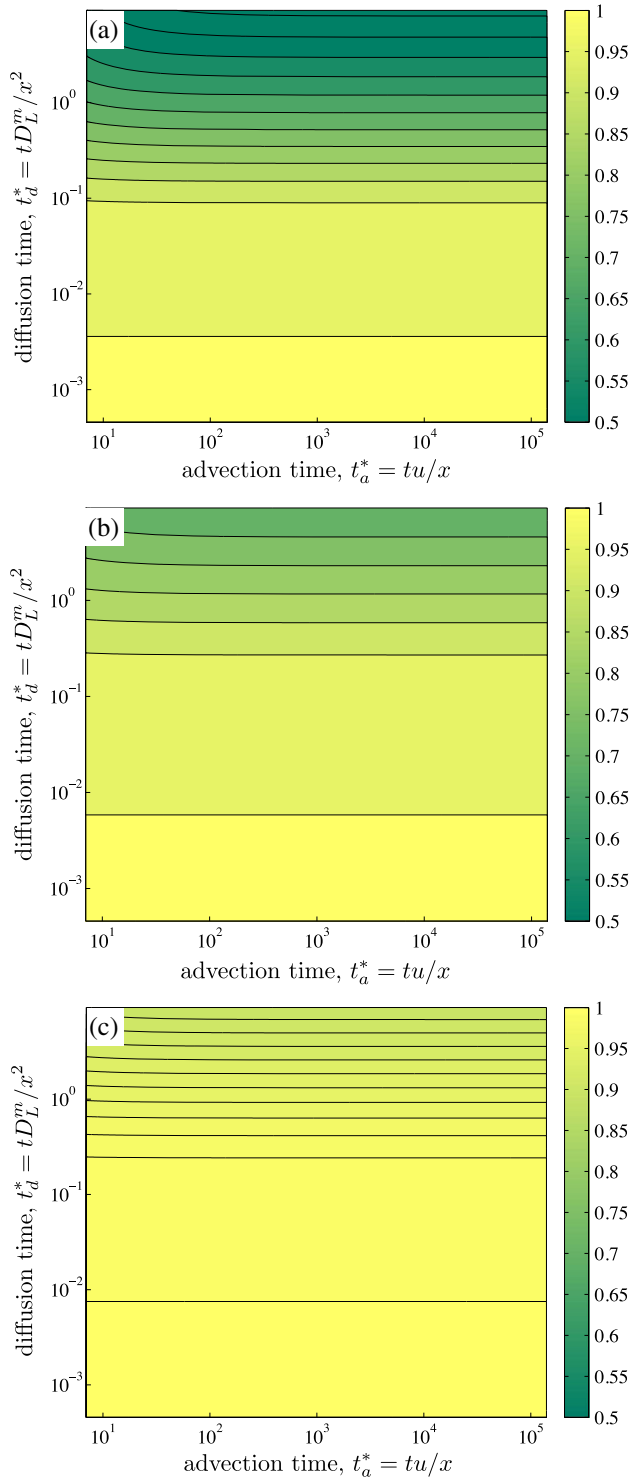

Figure 5. Isolines of the geothermal performance P_f in the space of advection (t_a^*) and diffusion (t_d^*) times, for (a) $R = 1$, (b) $R = 2$, and (c) $R = 5$.

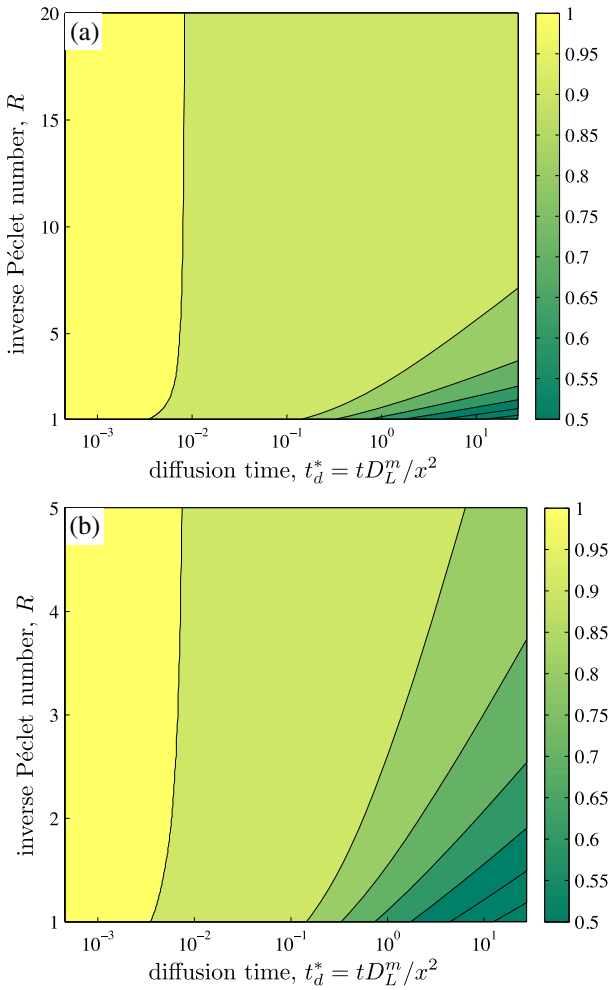

Figure 6. Isolines of the geothermal performance P_f in the space of diffusion time t_d^* and the inverse fracture-matrix Péclet number R, for (a) $1 \leq R \leq 20$ and (b) $1 \leq R \leq 5$.

fracture-matrix systems, i.e., enables one to decide whether a single-fracture-in-infinite-matrix model is sufficient or more evolved fracture-network models are to be used instead. Our 2-D solution, which accounts for longitudinal heat conduction in the matrix, demonstrates that heat sources in a fracture affect much smaller regions of the adjacent matrix than would be predicted with the classical 1-D solution, which ignores longitudinal conduction. Consequently, a conceptualization of heat dissipation in fractured rocks as a system of isolated fractures in infinite matrix might be adequate for geothermal studies.

5.2. Performance of Geothermal Systems

Relative temperature drawdown, $P_f(x,t) = 1 - T_r^f(x,t)$, is an effective performance measure of geothermal systems. It quantifies the degree to which temperature at a point x is affected (changes from initial temperature T_i) by injection of a fluid with temperature T_0 at another point (say, $x = 0$). The value $P_f = 0$ corresponds to zero cooling/heating efficiency (the fluid extracted at point x has the same temperature as that of the fluid injected at $x = 0$), and $P_f = 1$ represents the maximum cooling/heating efficiency (extracted fluid is at its initial temperature). Its values provide a consistent measure of performance regardless of whether the injected fluid is cooler ($T_0 < 0$) or warmer ($T_0 > 0$) than the host fluid.

Figure 5 exhibits $P_f(x,t)$ at $x = 10$ m for flow velocity $u = 1.4 \times 10^{-3}$ m/s and fracture aperture $2b = 10^{-3}$ m (Figure 5a), 5×10^{-4} (Figure 5b), and 2×10^{-4} m (Figure 5c). These aperture values translate into the inverse fracture-matrix Péclet number $R = 1$, 2, and 5, respectively. Isolines of $P_f(x,t)$ are plotted as a function of advection ($t_a^* = tu/x$) and diffusion ($t_d^* = tD_L^m/x^2$) times. This corresponds to physical time t ranging from 5×10^4 s to 10^9 s (from hours to 30 years).

Geothermal performance increases with R: it is lowest in the advection-dominated regime (Figure 5a) and highest in the diffusion-dominated regime (Figure 5c). In a given regime (as characterized by the value of R), the performance varies only slightly with t_a^*, i.e., it is relatively insensitive to convective properties of fractured rocks. This is to be expected from Figure 4, which shows that temperature in the fracture stabilizes quickly as the advection time t_a^* increases, so that subsequent increases in t_a^* have a limited impact on system performance.

When $R = \mathcal{O}(1)$, the geothermal performance P_f depends strongly on the diffusion time t_d^*, with high performance occurring at small values of t_d^*. Therefore, the cooling/heating efficiency increases with the reservoir size (the distance x between fluid's injection and extraction) and decreases with exploitation time t. As R increases (from $R = 1$ in Figure 5a to $R = 5$ in Figure 5c), the dependence of the geothermal performance P_f on t_d^* diminishes, leading to stable and efficient configurations in the diffusion-dominated regime. For large values of t_d^* (the top of Figures 5a–5c), the geothermal performance is slightly higher at small values of t_a^*. This implies that for rocks with large thermal diffusivity D_L^m (large values of t_d^*), the largest changes in fluid temperature in the fracture occur at early times t_a and the geothermal performance can be improved by decreasing flow velocity u.

Figure 6 illustrates these points further. Extracted fluid remains at its initial temperature regardless of the temperature of injected fluid for $t_d^* < 10^{-2}$. The latter inequality holds for small values of D_L^m, short exploitation times t, and/or large distances (x) between the injection and extraction points. This nearly perfect geothermal performance ($P_f > 0.9$) is observed when $R > 7$. In other words, the diffusion-dominated regime is best suited for geothermal exploitation, since it limits the thermal impact of injected fluids on the host fluid in a fracture by maximizing heat dissipation into the matrix. In the advection-dominated regime with $R < 5$ (Figure 6b), the geothermal performance depends strongly on t_d^*, with small values of t_d^* (short exploitation times t or/and large injection-to-extraction distances x) improving P_f.

6. Conclusions

We developed analytical models for heat transfer in a single fracture surrounded by an infinite matrix. These models account for advection and hydrodynamic dispersion in the fracture, longitudinal and transverse conduction in the matrix, and a two-way coupling between heat transfer in the fracture and matrix. They also handle any heat source configuration, such as distributed or localized heat sources of arbitrary duration.

In their most general form, these solutions are given by their Fourier and Laplace transforms and require numerical inversion. Under conditions that are typical of geothermal reservoirs, these solutions are inverted analytically, giving rise to an explicit closed-form model of heat transfer in fractured rocks. By accounting for two-dimensional heat conduction in rock matrix, this model represents a significant advance over the existing analytical solutions that restrict matrix conduction to the direction perpendicular to the fracture. Our analysis leads to the following major conclusions.

1. Longitudinal thermal diffusivity in the matrix is a critical parameter that determines the impact of local heat sources on fluid temperature in the fracture.
2. By neglecting longitudinal conduction in the matrix, the classical models significantly overestimate both fracture temperature and time-to-equilibrium.
3. The inverse fracture-matrix Péclet number R and diffusion timescale t_d^* are two parameters that determine the efficiency of geothermal systems.
4. The diffusion-dominated regime ($R > 7$) is ideal for geothermal exploitation, since it limits the thermal impact of injected fluids on the host fluid in a fracture by maximizing heat dissipation into the matrix.
5. In the advection-dominated regime ($R < 5$), the geothermal performance depends strongly on t_d^*. It is highest at small values of t_d^* (short exploitation times and/or large injection-to-extraction distances).

Our analytical models provide an easy-to-use tool for parametric sensitivity analysis, benchmark studies, and validation of numerical simulations. They can be used for geothermal site evaluation and parameter identification. They will improve field-scale studies of geothermal reservoirs, which rely on discrete fracture network approaches and consider only one-dimensional heat conduction in the rock. Our solutions obviate the need for this strong and limiting assumption, while retaining the analytic simplicity of the original approaches.

In the follow-up studies, we will generalize these analytical models by incorporating the following phenomena.

1. Fracture wall roughness. The numerical simulations of *Neuville et al.* [2010] demonstrated the effects of fracture wall roughness on heat transfer in fractured rocks. Treating fracture walls as random fields, and combining our solutions with stochastic domain mappings [*Xiu and Tartakovsky*, 2006; *Tartakovsky and Xiu*, 2006; *Park et al.*, 2012] and stochastic homogenization [*Tartakovsky et al.*, 2003], will enable us to investigate these effects in a computationally efficient semi-analytical manner. The latter step will rely on the Green's functions derived in this study.
2. Heat transfer in fracture networks. Multiscale modeling approaches to flow and transport in fractured rocks [e.g., *Dershowitz and Miller*, 1995; *Cvetkovic et al.*, 2004; *Roubinet et al.*, 2010, 2013] combine a discrete fracture network (DFN) representation at the field scale with analytical solutions at the fracture scale. We will embed our analytical solutions into particle-tracking DFN models to represent rock conduction effects at the field scale with optimized computational cost and representation accuracy.

Appendix A: Green's Functions

A1. Green's Function for Fracture BVP

We represent the two-dimensional Green's function G^f as the product of two one-dimensional Green's functions, $G^f = G^f_x(x;x';t-t')G^f_z(z;z';t-t')$ [*Carslaw and Jaeger*, 1959]

$$G^f_x = \frac{1}{2\sqrt{\pi D^f_L(t-t')}} \exp\left[\frac{-[x'-x+u(t-t')]^2}{4D^f_L(t-t')}\right] \tag{A1}$$

and

$$G^f_z = \frac{1}{b} + \frac{2}{b}\sum_{n=1}^{\infty} \mathrm{e}^{-\alpha_n^2 D^f_T(t-t')} \cos(\alpha_n z)\cos(\alpha_n z') \tag{A2}$$

where $\alpha_n = n\pi/b$. The Fourier Laplace (FL) transform of G^f has the form

$$\tilde{G}^f = \frac{\tilde{G}^f_\xi(s)}{\sqrt{2\pi}b} + \sqrt{\frac{2}{\pi}}\sum_{n=1}^{\infty} \frac{\cos(\alpha_n z)\cos(\alpha_n z')}{b} \tilde{G}^f_\xi(s+\alpha_n^2 D^f_T) \tag{A3}$$

where

$$\tilde{G}^f_\xi(s) = \frac{1}{s+\xi^2 D^f_L + u\xi i}. \tag{A4}$$

A2. Green's Function for Matrix BVP

The Green's function G^m is computed as the product of one-dimensional Green's functions, $G^m = G^m_x(x;x';t-t')G^m_z(z;z';t-t')$,

$$G^m_x = \frac{1}{2\sqrt{\pi D^m_L(t-t')}} \exp\left[\frac{-(x'-x)^2}{4D^m_L(t-t')}\right] \tag{A5}$$

and

$$G^m_z = \frac{\mathrm{e}^{-(z'-z)^2/\omega} + \mathrm{e}^{-(z'+z-2b)^2/\omega}}{2\sqrt{\pi D^m_T(t-t')}} \tag{A6}$$

where $\omega = 4D^m_T(t-t')$. The FL transform of G^m is

$$\tilde{G}^m = \frac{\mathrm{e}^{-\psi|z-z'|/\sqrt{D^m_T}} + \mathrm{e}^{-\psi|z+z'-2b|/\sqrt{D^m_T}}}{2\sqrt{2\pi D^m_T}\psi} \tag{A7}$$

where $\psi = \sqrt{D^m_L\xi^2 + s}$.

Appendix B: Integral Solutions of BVPs

Solutions of the fracture and matrix BVPs, expressed in terms of the Green's functions, are

$$T^f(x,z,t) = \int_0^t \int_{-\infty}^{\infty} r(x',t')G^f(.;x',b;.)\mathrm{d}x'\mathrm{d}t' + \int_0^t \int_0^b \int_{-\infty}^{\infty} f(x',z',t')G^f(.;.;.)\mathrm{d}x'\mathrm{d}z'\mathrm{d}t' \tag{B1}$$

and

$$T^m(x,z,t) = -\frac{1}{\phi_m}\int_0^t \int_{-\infty}^{\infty} r(x',t')G^m(.;x',b;.)\mathrm{d}x'\mathrm{d}t'. \tag{B2}$$

Their FL transforms are

$$\tilde{T}^f = \sqrt{2\pi}\left(\tilde{r}\tilde{G}^f|_{z'=b} + \int_0^b \tilde{f}\tilde{G}^f\mathrm{d}z'\right) \tag{B3}$$

$$\tilde{T}^m = -\frac{\sqrt{2\pi}\tilde{r}\tilde{G}^m|_{z'=b}}{\phi_m}, \tag{B4}$$

where $\tilde{G}^f$ and $\tilde{G}^m$ are given by (A3) and (A7), respectively.

The FL transform of the fracture-matrix heat transfer, $\tilde{r}(\xi,s)$, is obtained from the continuity condition at the interface, $\tilde{T}^f(\xi,z=b,s) = \tilde{T}^m(\xi,z=b,s)$.

Appendix C: Fourier-Laplace Inversions

Since $\tilde{T}^f(\xi,s) = \tilde{T}^*(-\xi,s)$ (where $\tilde{T}^*$ denotes the conjugate of $\tilde{T}^f$), the inverse Fourier transform of $\tilde{T}^f$ is

$$\bar{T}^f = \frac{1}{\sqrt{2\pi}}\int_0^{\infty}\left[\tilde{T}^*(\xi,s)\mathrm{e}^{-ix\xi} + \tilde{T}^f(\xi,s)\mathrm{e}^{ix\xi}\right]\mathrm{d}\xi \tag{C1}$$

and its inverse Laplace transform is

$$T^f = \frac{1}{\sqrt{2\pi}}\int_0^{\infty}\left[L^{-1}[\tilde{T}^*]\mathrm{e}^{-ix\xi} + L^{-1}[\tilde{T}^f]\mathrm{e}^{ix\xi}\right]\mathrm{d}\xi \tag{C2}$$

where $L^{-1}[\ ]$ represents the inverse Laplace operator.

C1. Inverse Laplace Transform of $\tilde{T}^f$

We decompose the FL transform $\tilde{T}^f$ in (11) into simple fractions

$$\tilde{T}^f = A\sum_{i=1}^{4}\frac{X_i}{\psi + b_i}, \qquad A = \frac{T_0 u}{\sqrt{2\pi}} \tag{C3}$$

where $b_1 = B/2 + \sqrt{G - Di}$, $b_2 = B/2 - \sqrt{G - Di}$, $b_3 = -b_4 = \sqrt{C}$, $X_1 = 1/[(b_1 - b_2)(C - b_1^2)]$, $X_2 = -1/[(b_1 - b_2)(C - b_2^2)]$, $X_3 = -1/\{2\sqrt{C}[(C + b_1 b_2) - (b_1 + b_2)\sqrt{C}]\}$, $X_4 = 1/\{2\sqrt{C}[(C + b_1 b_2) + (b_1 + b_2)\sqrt{C}]\}$, and

$$B = \frac{\phi_m\sqrt{D_T^m}}{b}, \quad C = D_L^m\xi^2, \quad D = u\xi, \quad G = \frac{B^2}{4} + C. \tag{C4}$$

Since only $\psi = \sqrt{C + s}$ depends on the Laplace variable s, and noticing that $\sum_{i=1}^{4} X_i = 0$, the inverse Laplace of $\tilde{T}^f$ is

$$\hat{T}^f = -A\mathrm{e}^{-Ct}\sum_{i=1}^{4} X_i b_i \mathrm{e}^{b_i^2 t}\mathrm{erfc}(b_i\sqrt{t}) \tag{C5}$$

which can be recast in terms of the function $w(z) = e^{-z^2}\mathrm{erfc}(-iz)$ of a complex variable z [*Faddeeva and Terent'tev*, 1961] as

$$\begin{aligned}\hat{T}^f = &\frac{AB\sqrt{C}}{B^2C+D^2}\left[1-\mathrm{erfc}(\sqrt{Ct})\right]\\ &-\frac{ADi}{B^2C+D^2}\left[1-e^{-Ct}w(ib_1\sqrt{t})\right]\\ &+AX_2b_2e^{-Ct}\left[w(ib_1\sqrt{t})-w(ib_2\sqrt{t})\right].\end{aligned} \tag{C6}$$

C2. Inverse Fourier Transform of $\hat{T}^f$

Recalling that b_1 and b_2 in (C6) are given by

$$b_1 = \frac{B}{2}+\sqrt{\frac{\sqrt{G^2+D^2}+G}{2}}-i\sqrt{\frac{\sqrt{G^2+D^2}-G}{2}} \tag{C7}$$

$$b_2 = \frac{B}{2}-\sqrt{\frac{\sqrt{G^2+D^2}+G}{2}}+i\sqrt{\frac{\sqrt{G^2+D^2}-G}{2}}, \tag{C8}$$

expanding the square roots into Taylor series, and requiring $G \gg D$ leads to

$$b_1 \approx \frac{B}{2}+\sqrt{G+\frac{D^2}{4G}}-\frac{iD}{2\sqrt{G}}, \qquad b_2 \approx \frac{B}{2}-\sqrt{G+\frac{D^2}{4G}}+\frac{iD}{2\sqrt{G}}. \tag{C9}$$

Requiring $B^2/4 \gg C$, and expanding the square roots into Taylor series, yields

$$b_1 \approx B-i\frac{D}{B}, \qquad b_2 \approx -\frac{C}{B}-\frac{D^2}{B^3}+i\frac{D}{B}. \tag{C10}$$

Similarly, X_2b_2 in (C6) is approximated by

$$X_2b_2 \approx \frac{1}{B^2}-\frac{iD}{B^2C+D^2}. \tag{C11}$$

Finally, for small values of ξ, we approximate b_1 and b_2 in the arguments of $w(\cdot)$ with $b_1 \approx B$ and $b_2 \approx iD/B$, so that

$$\begin{aligned}w(ib_1\sqrt{t}) &\approx e^{B^2t}\mathrm{erfc}(B\sqrt{t})\\ w(ib_2\sqrt{t}) &\approx e^{-D^2t/B^2}\mathrm{erfc}(iD\sqrt{t}/B).\end{aligned} \tag{C12}$$

For $t > 10^4/B^2$, expanding $\mathrm{erfc}(iD\sqrt{t}/B)$ into a Taylor series yields

$$\begin{aligned}w(ib_1\sqrt{t}) &\approx 0\\ w(ib_2\sqrt{t}) &\approx e^{-\epsilon^2}\left[1-\left(\frac{2}{\sqrt{\pi}}\epsilon+\frac{2}{3\sqrt{\pi}}\epsilon^3+\frac{1}{5\sqrt{\pi}}\epsilon^5\right)i\right],\end{aligned} \tag{C13}$$

where $\epsilon = D\sqrt{t}/B$. With these approximations, (C6) is replaced with

$$\hat{T}^f \approx \frac{A\sqrt{C}}{B^2\kappa}\mathrm{erf}(\sqrt{Ct})-\frac{ADi}{B^2\kappa}-\frac{A(\kappa-Di)}{B^2\kappa}\left[1-\left(\frac{2\epsilon}{\sqrt{\pi}}+\frac{2\epsilon^3}{3\sqrt{\pi}}+\frac{\epsilon^5}{5\sqrt{\pi}}\right)i\right]e^{-\kappa t} \tag{C14}$$

where $\kappa = C + D^2/B^2$. Using (C2) to compute the inverse Fourier transform leads to (13).

C3. Limits of Applicability of Analytical Model (13)

The Fourier transform of temperature in the fracture (C14) and its exact analytical inversion (13) are derived under the following three conditions:

1. $B^2/4 + C \gg D$
2. $B^2/4 \gg C$
3. $t > 10^4/B^2$.

In what follows, we demonstrate the general applicability of these conditions.

Condition 1: Solving the first condition $B^2/4 + C \gg D$ as an equation results in

$$\xi^2 = \frac{u^2}{2D_L^{m2}} - \frac{\phi_m^2 D_T^m}{4b^2 D_L^m} \pm \frac{u}{2D_L^{m2}}\sqrt{u^2 - \frac{\phi_m^2 D_L^m D_T^m}{b^2}}. \tag{C15}$$

Thus, ξ is real if

$$\frac{\phi_m \sqrt{D_L^m D_T^m}}{ub} > 1. \tag{C16}$$

Condition 2: Recalling (C4), this condition implies $\xi^2 \ll \phi_m^2 D_T^m/(4D_L^m b^2)$. When $\xi > 1$, this is equivalent to $\xi < \phi_m\sqrt{D_T^m/D_L^m}/(2b)$, which gives

$$\frac{\phi_m}{2b}\sqrt{\frac{D_m^T}{D_m^L}} > 1. \tag{C17}$$

Condition 3: For $B^2 t = 10^4$, $e^{B^2 t}\mathrm{erfc}(\sqrt{B^2 t}) \approx 0.0056$ and we treat it as 0. This yields a third constraint,

$$t > \frac{10^4 b^2}{\phi_m^2 D_T^m}. \tag{C18}$$

Acknowledgments
This work was supported in part by the National Science Foundation award EAR-1246315 and by the Computational Mathematics Program of the Air Force Office of Scientific Research.

References

Al-Hadhrami, H. S., and M. J. Blunt (2001), Thermally induced wettability alteration to improve oil recovery in fractured reservoirs, *SPE Reserv. Eval. Eng.*, *4*(3), 179–186.

Baston, D. P., and B. H. Kueper (2009), Thermal conductive heating in fractured bedrock: Screening calculations to assess the effect of groundwater influx, *Adv. Water Resour.*, *32*, 231–238.

Bataillé, A., P. Genthon, M. Rabinowicz, and B. Fritz (2006), Modeling the coupling between free and forced convection in a vertical permeable slot: Implications for the heat production of an enhanced geothermal system, *Geothermics*, *35*, 654–682.

Bodvarsson, G. S., and C. F. Tsang (1982), Injection and thermal breakthrough in fractured geothermal reservoirs, *J. Geophys. Res.*, *87*(NB2), 1031–1048.

Carslaw, H. S., and J. C. Jaeger (1959), *Conduction of Heat in Solids*, Oxford Univ. Press, New York.

Chen, X., and P. M. Shearer (2011), Comprehensive analysis of earthquake source spectra and swarms in the Salton Trough, California, *J. Geophys. Res.*, *116*, B09309, doi:10.1029/2011JB008263.

Cheng, A. H.-D., A. Ghassemi, and E. Detournay (2001), Integral equation solution of heat extraction from a fracture in hot dry rocks, *Int. J. Numer. Anal. Methods Geomech.*, *25*(13), 1327–1338.

Cvetkovic, V., S. Painter, N. Outters, and J. O. Selroos (2004), Stochastic simulation of radionuclide migration in discretely fractured rock near the Aspo Hard Rock Laboratory, *Water Resour. Res.*, *40*, W02404, doi:10.1029/2003WR002655.

de Hoog, F. R., J. H. Knight, and A. N. Stokes (1982), An improved method for numerical inversion of Laplace transforms, *SIAM J. Sci. Comput.*, *3*(3), 357–366.

Dershowitz, W., and I. Miller (1995), Dual-porosity fracture flow and transport, *Geophys. Res. Lett.*, *22*(11), 1441–1444.

Faddeeva, V. N., and N. M. Terent'tev (1961), *Tables of Values of the Function w(z) for Complex Argument*, Pergamon Press, New York.

Gelet, R., B. Loret, and N. Khalili (2012), A thermo-hydro-mechanical coupled model in local thermal non-equilibrium for fractured HDR reservoir with double porosity, *J. Geophys. Res.*, *117*, B07205, doi:10.1029/2012JB009161.

Gringarten, A. C., P. A. Witherspoon, and Y. Ohnishi (1975), Theory of heat extraction from fractured hot dry rock, *J. Geophys. Res.*, *80*(8), 1120–1124.

Gunasekera, R. C., G. R. Foulger, and B. R. Julian (2003), Reservoir depletion at The Geysers geothermal area, California, shown by four-dimensional seismic tomography, *J. Geophys. Res.*, *108*(B3), 2134, doi:10.1029/2001JB000638.

Kolditz, O. (1995), Modeling flow and heat-transfer in fractured rocks: Dimensional effect of matrix heat diffusion, *Geothermics*, *24*(3), 421–437.

Lin, W. (2002), Permanent strain of thermal expansion and thermally induced microcracking in Inada granite, *J. Geophys. Res.*, *107*(B10), 2215, doi:10.1029/2001JB000648.

Meyer, J. (2004), Development of a heat transport analytical model for a single fracture in a porous matrix, Report for Earth 661, University of Waterloo.

Molson, J., P. Pehme, J. Cherry, and B. Parker (2007), Numerical analysis of heat transport within fractured sedimentary rock: Implications for temperature probes, paper presented at NGWA/U.S.EPA Fractured Rock Conference: State of the Science and Measuring Success in Remediation, vol. 5017, Portland, Maine.

Neuville, A., R. Toussaint, and J. Schmittbuhl (2010), Hydrothermal coupling in a self-affine rough fracture, *82*, *036,317*, doi:10.1103/PhysRevE.82.036317.

Park, S.-W., M. Intaglietta, and D. M. Tartakovsky (2012), Impact of endothelium roughness on blood flow, *J. Theor. Biol.*, *300*, 152–160, doi:10.1016/j.jtbi.2012.01.017.

Pehme, P. E., J. P. Greenhouse, and B. L. Parker (2007), The active line source temperature logging technique and its application in fractured rock hydrogeology, *J. Environ. Eng. Geophys.*, *12*, 307–322.

Pehme, P. E., B. L. Parker, J. A. Cherry, and J. P. Greenhouse (2010), Improved resolution of ambient flow through fractured rock with temperature logs, *Ground Water*, *48*, 191–205.

Roubinet, D., H.-H. Liu, and J.-R. de Dreuzy (2010), A new particle-tracking approach to simulating transport in heterogeneous fractured porous media, *Water Resour. Res.*, *46*, W11507, doi:10.1029/2010WR009371.

Roubinet, D., J.-R. de Dreuzy, and D. M. Tartakovsky (2012), Semi-analytical solutions for solute transport and exchange in fractured porous media, *Water Resour. Res.*, *48*, W01542, doi:10.1029/2011WR011168.

Roubinet, D., J.-R. de Dreuzy, and D. M. Tartakovsky (2013), Particle-tracking simulations of anomalous transport in hierarchically fractured rocks, *Comput. Geosci.*, *50*, 52–58.

Sudicky, E. A., and E. O. Frind (1982), Contaminant transport in fractured porous-media: Analytical solutions for a system of parallel fractures, *Water Resour. Res.*, *18*(6), 1634–1642.

Tang, D. H., E. O. Frind, and E. A. Sudicky (1981), Contaminant transport in fractured porous-media: Analytical solution for a single fracture, *Water Resour. Res.*, *17*(3), 555–564.

Tartakovsky, D. M., and D. Xiu (2006), Stochastic analysis of transport in tubes with rough walls, *J. Comput. Phys.*, *217*, 248–259.

Tartakovsky, D. M., A. Guadagnini, and M. Riva (2003), Stochastic averaging of nonlinear flows in heterogeneous porous media, *J. Fluid Mech.*, *492*, 47–62, doi:10.1017/S002211200300538X.

Wang, H. F., B. P. Bonner, S. R. Carlson, B. J. Kowallis, and H. C. Heard (1989), Thermal-stress cracking in granite, *J. Geophys. Res.*, *94*(B2), 1745–1758.

Wang, J. S. Y., C. F. Tsang, N. G. W. Cook, and P. A. Witherspoon (1981), A study of regional temperature and thermohydrologic effects of an underground repository for nuclear wastes in hard rock, *J. Geophys. Res.*, *86*(NB5), 3759–3707.

Willis-Richards, J., K. Watanabe, and H. Takahashi (1996), Progress toward a stochastic rock mechanics model of engineered geothermal systems, *J. Geophys. Res.*, *101*(B8), 17,481–17,496.

Xiang, Y., and Y. Zhang (2012), Two-dimensional integral equation solution of advective-conductive heat transfer in sparsely fractured water-saturated rocks with heat source, *Int. J. Geomech.*, *12*, 168–175.

Xiu, D., and D. M. Tartakovsky (2006), Numerical methods for differential equations in random domains, *SIAM J. Sci. Comput.*, *28*(3), 1167–1185.

Xu, T. F., and K. Pruess (2001), On fluid flow and mineral alteration in fractured caprock of magmatic hydrothermal systems, *J. Geophys. Res.*, *106*(B2), 2121–2138.

Yang, S.-Y., and H.-D. Yeh (2009), Modeling heat extraction from hot dry rock in a multi-well system, *Appl. Therm. Eng.*, *29*, 1676–1681.

Zhou, Q., H.-H. Liu, F. J. Molz, Y. Zhang, and G. S. Bodvarsson (2007), Field-scale effective matrix diffusion coefficient for fractured rock: Results from literature survey, *J. Contam. Hydrol.*, *93*, 161–187.